Structural bases for the interaction and stabilization of the human amino acid transporter LAT2 with its ancillary protein 4F2hc

Albert Rosell[a,b,1], Marcel Meury[c,d,1], Elena Álvarez-Marimon[a,b,1], Meritxell Costa[a,b,c,d,1], Laura Pérez-Cano[e], Antonio Zorzano[a,f,g], Juan Fernández-Recio[e,2], Manuel Palacín[a,b,f,2], and Dimitrios Fotiadis[c,d,2]

[a]Institute for Research in Biomedicine (IRB Barcelona), E-08028 Barcelona, Spain; [b]Centro de Investigación Biomédica en Red de Enfermedades Raras, E-08028 Barcelona, Spain; [c]Institute of Biochemistry and Molecular Medicine, and [d]Swiss National Centre of Competence in Research TransCure, University of Bern, CH-3012 Bern, Switzerland; [e]Joint Barcelona Supercomputing Center-IRB Program in Computational Biology, Department of Life Sciences, Barcelona Supercomputing Center, E-08034 Barcelona, Spain; [f]Department of Biochemistry and Molecular Biology, Faculty of Biology, University of Barcelona, E-08028 Barcelona, Spain; and [g]Centro de Investigación Biomédica en Red de Diabetes y Enfermedades Metabólicas Asociadas, E-08028 Barcelona, Spain

Edited* by Christopher Miller, Howard Hughes Medical Institute, Brandeis University, Waltham, MA, and approved January 15, 2014 (received for review December 24, 2013)

Heteromeric amino acid transporters (HATs) are the unique example, known in all kingdoms of life, of solute transporters composed of two subunits linked by a conserved disulfide bridge. In metazoans, the heavy subunit is responsible for the trafficking of the heterodimer to the plasma membrane, and the light subunit is the transporter. HATs are involved in human pathologies such as amino acidurias, tumor growth and invasion, viral infection and cocaine addiction. However structural information about interactions between the heavy and light subunits of HATs is scarce. In this work, transmission electron microscopy and single-particle analysis of purified human 4F2hc/L-type amino acid transporter 2 (LAT2) heterodimers overexpressed in the yeast *Pichia pastoris*, together with docking analysis and crosslinking experiments, reveal that the extracellular domain of 4F2hc interacts with LAT2, almost completely covering the extracellular face of the transporter. 4F2hc increases the stability of the light subunit LAT2 in detergent-solubilized *Pichia* membranes, allowing functional reconstitution of the heterodimer into proteoliposomes. Moreover, the extracellular domain of 4F2hc suffices to stabilize solubilized LAT2. The interaction of 4F2hc with LAT2 gives insights into the structural bases for light subunit recognition and the stabilizing role of the ancillary protein in HATs.

CD98hc | 4F2hc ectodomain

Heteromeric amino acid transporters (HATs) are composed of two subunits, a heavy (SLC3 family) and a light subunit [SLC7 or L-type amino acid transporter (LAT) family] linked by a conserved disulfide bridge (1). HATs are amino acid exchangers (1), and this transport activity resides in the light subunit (2). The heavy subunit (either 4F2hc or rBAT) is essential for trafficking of the holotransporter to the plasma membrane (3, 4). In mammals, six transporters heterodimerize with 4F2hc, and only one heterodimerizes with rBAT. The rBAT/$b^{0,+}$AT complex is a dimer of heterodimers in which the light subunit is required for proper rBAT folding and stability (5, 6). In contrast, 4F2hc-associated transporters are simple heterodimers (6), and possible stabilizing roles of the two subunits in the biogenesis of the heterodimer have not been described.

HATs have major impacts on human health and are involved directly in amino acidurias (cystinuria and lysinuric protein intolerance), tumor cell growth, glioma invasion, Kaposi's sarcoma-associated herpesvirus infection, and cocaine relapse (1). In addition to the role of HATs in amino acid transport, 4F2hc heterodimers mediate β1- and β3-integrin signaling (7).

Structural information about HATs is scarce (1). The heavy subunits are type II membrane *N*-glycoproteins with a single transmembrane domain (TMD), an intracellular N terminus, and a large extracellular C terminus with sequence homology with bacterial α-amylases. Indeed, the atomic structure of the extracellular domain (ED) of human 4F2hc (4F2hc-ED) is similar to that of bacterial glucosidases [i.e., a triose phosphate isomerase barrel, $(\beta\alpha)_8$, (subdomain A) and eight antiparallel β-strands (subdomain C)] but lacks glucosidase activity (8). The conserved cysteine residue participating in the intersubunit disulfide bridge is located between the single TMD and 4F2hc-ED. Physical and functional interaction of 4F2hc with integrins has been mapped to the TMD and cytosolic N-terminal domain (7, 9), whereas 4F2hc-ED is necessary for functional heterodimerization with the light subunit (9, 10). The light subunits are nonglycosylated proteins and have a 12-TMD topology with intracellular N and C termini (1). The conserved cysteine residue involved in the intersubunit disulfide bridge is located between TMD3 and TMD4 (11). Structure–function studies (12, 13) suggest that the structures of the light subunit of HATs should be similar to those of remote bacterial amino acid/polyamine/organocation (APC) transporters (~20% amino acid sequence identities), which present the LeuT-fold (14–17). In contrast, there is no structural information about the interaction between the two HAT subunits. In the present study, we show that information from transmission electron microscopy (TEM) and single-particle analysis (SPA) of human 4F2hc/L-type amino acid transporter 2 (LAT2) heterodimers is compatible with 4F2hc-ED interacting with the extracellular loops of LAT2. Docking analyses and crosslinking experiments indicated a location of 4F2hc-ED almost completely covering the external face of LAT2. Moreover, 4F2hc increases the stability of detergent-solubilized

Significance

Here we report the structural bases of the interaction between the catalytic light subunit and the heavy subunit of the heteromeric amino acid transporters. Our data show that the large ectodomain of the human heavy subunit 4F2hc plays a key role in the interaction and stability of the light subunit L-type amino acid transporter 2. This finding paves the way for structural and functional studies to elucidate the role of the heavy subunit in the regulation of these transporters; such studies will be highly relevant in human pathology.

Author contributions: A.R., M.M., E.Á.-M., M.C., L.P.-C., J.F.-R., M.P., and D.F. designed research; A.R., M.M., E.Á.-M., M.C., and L.P.-C. performed research; A.R., M.M., E.Á.-M., M.C., L.P.-C., A.Z., J.F.-R., M.P., and D.F. analyzed data; and J.F.-R., M.P., and D.F. wrote the paper.

The authors declare no conflict of interest.

*This Direct Submission article had a prearranged editor.

[1]A.R., M.M., E.Á.-M., and M.C. contributed equally to this work.

[2]To whom correspondence may be addressed. E-mail: juanf@bsc.es, manuel.palacin@irbbarcelona.org, or dimitrios.fotiadis@ibmm.unibe.ch.

This article contains supporting information online at www.pnas.org/lookup/suppl/doi:10.1073/pnas.1323779111/-/DCSupplemental.

LAT2, allowing functional reconstitution of the heterodimer into proteoliposomes. The interaction of 4F2hc-ED with LAT2 provides insights regarding the structural bases for recognition of the light subunit and the stabilization of this complex and other 4F2hc associated transporters.

Results

TEM, SPA, and 3D Reconstruction of the Human 4F2hc/LAT2 Complex. Recombinant 4F2hc/LAT2 purified by Co^{2+}- and Strep-Tactin affinity chromatography (18) was analyzed by negative-stain TEM and SPA to unveil the supramolecular architecture of HATs (Fig. 1). On electron micrographs distinct particles corresponding to purified 4F2hc/LAT2 complexes are discerned as composed of two globular domains of different sizes (Fig. 1*A*, boxed particles and gallery). From 15,210 single-particle projections, class averages were calculated (Fig. S1*A*). Most class averages indicate a clear difference in size between the two domains. A few smaller particles reflecting 4F2hc or LAT2 from disrupted heterodimers were also found on electron micrographs (Fig. 1*A*, arrowheads). In addition, some small protein aggregates are seen on electron micrographs (Fig. 1*A*, asterisks). We determined the structure of 4F2hc/LAT2 by 3D reconstruction from negatively stained complexes (Fig. 1*B*). The resolution of the 3D map obtained from the final refinement run was 21 Å (Fig. S1*B*) and had a homogeneous angular distribution of projections (Fig. S1*C*). The calculated 3D map reflects a structure composed of a smaller and a larger density (Fig. 1*B*; see Fig. S1*D* for additional views). The smaller domain lies tilted (not flat) on the larger domain (Fig. 1*B*, black dotted line). Consequently, the complex has a cleft on one side (Fig. 1*B*, arrowhead) and a seal on the opposite side (Fig. 1*B*, white dotted curve). Importantly, the crystal structure of 4F2hc-ED fits nicely into the smaller density (Fig. 1*C*), making the assignment of 4F2hc and LAT2 in the 3D map possible. As determined by scanning TEM mass measurement, unstained n-dodecyl-β-D-maltoside (DDM)-purified membrane proteins prepared in a conventional way for TEM are associated with >55 kDa of copurified endogenous lipids and DDM molecules (19). Thus, the total mass of the LAT2/lipid/DDM ternary complex plus the single TMD and the cytoplasmic N-terminal domain of 4F2hc containing the His-tag and the protease cleavage site (>120 kDa) is significantly larger than that of the 4F2hc-ED (~50 kDa). This result, together with the fitting of the 4F2hc crystal structure into the smaller density, supports the assignment of LAT2 to the larger domain of the 3D map. In Fig. 1*C* the location of the N terminus in the 4F2hc-ED crystal structure is marked by an asterisk. This location is close to an additional density connecting the small and large domains that possibly arises from the N-terminal TMD of 4F2hc and extracellular loops of LAT2.

Crosslinking of 4F2hc-ED and LAT2. To confirm the interaction between 4F2hc-ED and LAT2, specific intersubunit crosslinking between cysteine residues were assessed in purified 4F2hc/LAT2 heterodimers (Fig. 2). To this end, homogenates from HEK293T cells transiently cotransfected with N-terminally His-tagged 4F2hc (His-4F2hc) and N-terminally Strep-TagII–tagged LAT2 (Strep-LAT2) were solubilized with DDM and purified by Ni^{2+}-affinity chromatography and then were crosslinked with the nonreducible cysteine crosslinkers bis(maleimido)ethane (BMOE) (with a spacer arm up to 10.5 Å) or 1,8-bis(maleimido)diethylene glycol [$BM(POE)_2$] (with a spacer arm up to 14.3 Å). Crosslinking experiments were performed in mammalian cells because mutants could be generated more conveniently in mammalian cells than in *Pichia* cells. Western blotting under reducing conditions and using an anti-Strep antibody revealed intersubunit crosslinking as DTT-resistant heterodimers. Human 4F2hc has two cysteine residues: Cys109, participating in the intersubunit disulfide bridge (located in the "neck" connecting the TMD and ectodomain) and Cys330, a partially hidden residue (located in the A-subdomain of the ectodomain). To avoid doubtful results, residue Cys330 was mutated to serine (C330S) in all mutants studied, and residue Cys109 was maintained to hold the disulfide intersubunit bridge. This strategy was validated by demonstrating heterodimerization of His-4F2hc C330S with Strep-LAT2 and induction of L-alanine transport in HEK293T cells (Fig. S2 *A–D*).

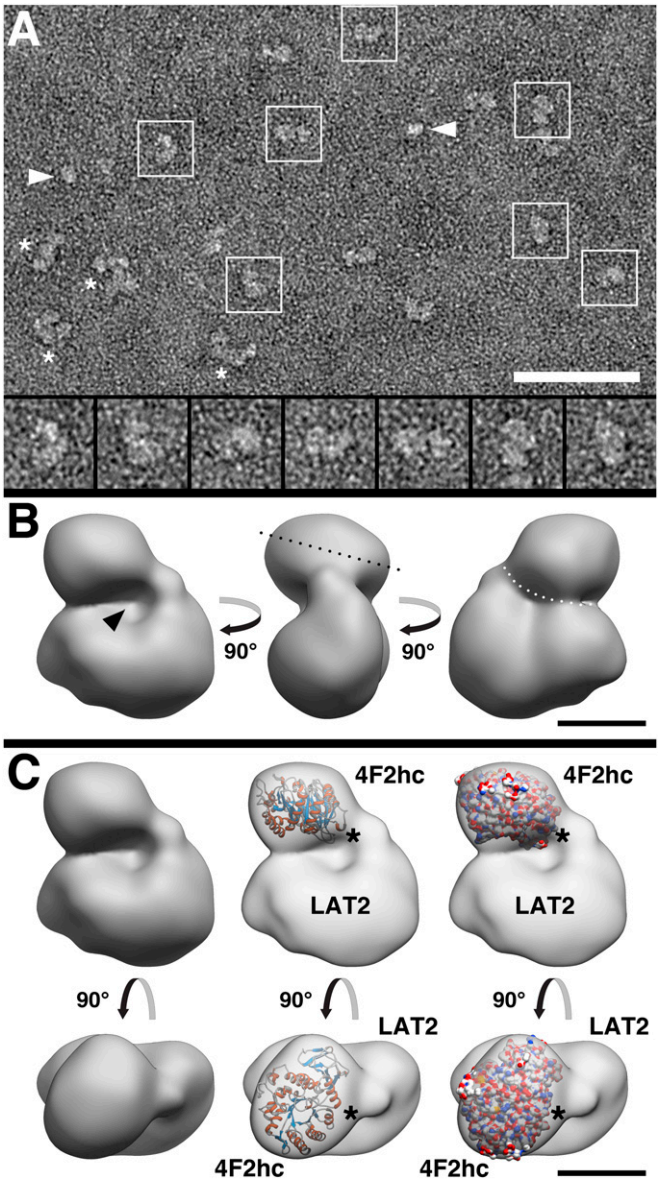

Fig. 1. TEM, SPA, and 3D reconstruction of human 4F2hc/LAT2. (*A*) Overview electron micrograph of purified, negatively stained 4F2hc/LAT2 heterodimers. The boxed 4F2hc/LAT2 complexes were magnified and are displayed in the gallery. Arrowheads mark 4F2hc or LAT2 monomers from disrupted heterodimers. Asterisks indicate small protein aggregates. (Scale bar: 50 nm.) The frame sizes of the magnified particles in the gallery are 21.8 nm. (*B*) 3D reconstruction of 4F2hc/LAT2 calculated from projections of negatively stained heterodimer particles. Different side views of the 3D model are shown. 4F2hc/LAT2 is composed of a large and a small density. The small density is located on top of the large density and is tilted, as indicated by the black dotted line. As indicated by an arrowhead, the 3D model features a distinct cavity. On the opposite side, both subunits are in close contact, as marked by the white, dotted curve. (Scale bar: 5 nm.) (*C*) Side (*Upper*) and top (*Lower*) views of the 4F2hc/LAT2 3D reconstruction without and with the fitted crystal structure of the 4F2hc-ED (Protein Data Bank ID code: 2DH2). The fitting assigns the small and large subunits to 4F2hc and LAT2, respectively. The structure of 4F2hc-ED is represented as a cartoon and surface model. Asterisks indicate the location of the N terminus in the 4F2hc-ED crystal structure. (Scale bar: 5 nm.)

BIOCHEMISTRY

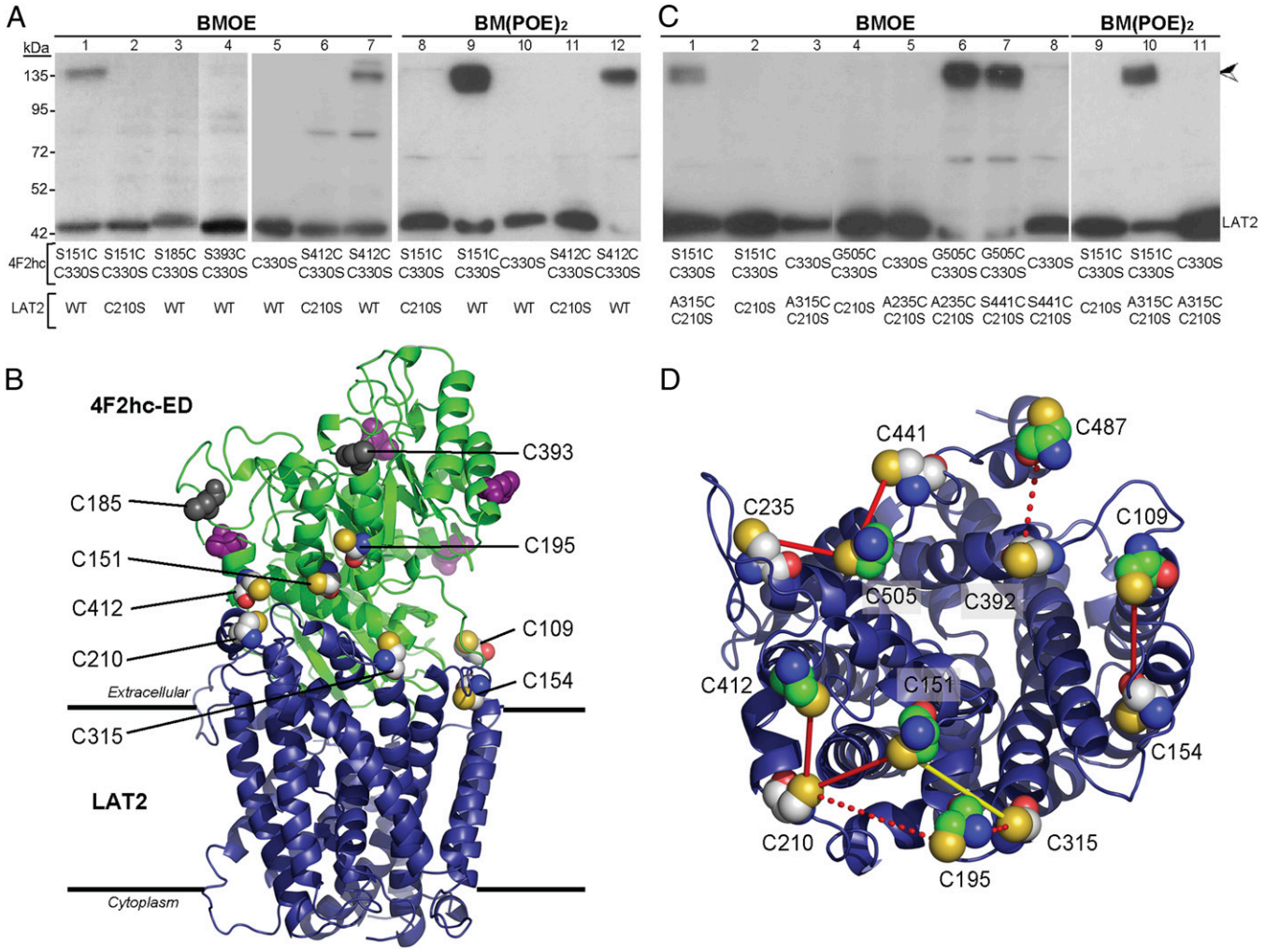

Fig. 2. Crosslinking of 4F2hc/LAT2 and docking model of the 4F2hc-ED and LAT2 complex. (*A* and *C*) Intersubunit crosslinking. Versions of His-4F2hc/Strep-LAT2 heterodimers expressed in HEK293T cells and purified by His-affinity chromatography were treated with the DTT-uncleavable crosslinkers BMOE or BM(POE)$_2$. Crosslinking was detected as DTT-resistant 4F2hc/LAT2 heterodimers (arrowhead) by Western blotting using αStrep antibodies under reducing conditions. The band of LAT2 monomer corresponds to LAT2 forming heterodimers with 4F2hc (i.e., copurified but not crosslinked). Single cysteine mutants were introduced in 4F2hc (C330S)/LAT2 wild-type (*A*) or LAT2 (C210S) (*C*). In all cases, crosslinking was abolished when 4F2hc (C330S) or LAT2 (C210S) was used, indicating the specificity of the crosslinked sites. (*B*) Lowest-energy model of the 4F2hc-ED–LAT2 complex. Highlighted cysteine residues (endogenous or added through mutation) are shown as sphere models (C atoms, gray; O atoms, red; N atoms, blue; S atoms, yellow). The putative *N*-glycosylation sites (N264, N280, N323, and N405 indicated in purple) and the non-crosslinked residues (C185 and C393 in gray) of 4F2hc are located in the most external face. (*D*) Summary of the crosslinked residues. The 4F2hc-ED–LAT2 model in *B* was rotated by 90°, i.e., viewed from 4F2hc-ED. Only the cysteine residues (endogenous or added through mutation) of the 4F2hc-ED are shown as sphere models with C atoms in green. In LAT2 (cartoon in blue) the cysteine residues (endogenous or added through mutation) are shown as sphere models with C atoms in gray. Crosslinked residues are connected by a line denoting the percentage of crosslinking (solid red line: 80–95%; solid yellow line: ∼60%; red dotted line: 5–10%). Similarly, the intersubunit disulfide bridge between C109 (4F2hc) and C154 (LAT2) is represented by a solid red line because it is present in >95% of the expressed LAT2 (see text for details).

According to our homology models of human LAT2 (Fig. S3 *A* and *B*), which are based on the atomic structure of the bacterial L-arginine/agmatine exchanger AdiC (17), seven of the nine endogenous cysteine residues in LAT2 are located in TMDs and internal loops (Fig. S3 *A* and *C*). The remaining two cysteine residues are in external loops: Cys154, participating in the intersubunit disulfide bridge, is located in the external loop TMD3–4, and Cys210 is located in the external loop TMD5–6 (Fig. S3 *A* and *C*). Nine serine residues spread over the surface of 4F2hc-ED potentially facing LAT2 (8) were selected and mutated individually to cysteine for crosslinking experiments (see locations in Fig. S2*E*). Five of the nine mutants were not considered for further studies because they produced proteolyzed proteins (S191C and S200C) (Fig. S2*F*, lanes 2 and 3) or lacked (S270C) (Fig. S2*F*, lane 4) or inefficiently formed (S497C and S506C) (Fig. S2 *G* and *H*, lanes 7 and 8) intersubunit disulfide bridges when cotransfected with Strep-LAT2. The other four 4F2hc mutants (S151C, S185C, S393C, and S412C), also containing the C330S mutation, heterodimerized with Strep-LAT2 (Fig. S2 *G* and *H*, lanes 1, 3, 5, and 6) and induced L-alanine transport similar to 4F2hc C330S (Fig. S2*I*). Of these four mutants, only S151C and S412C could be crosslinked with wild-type LAT2 using BMOE and BM(POE)$_2$ [Fig. 2*A*; BMOE: lanes 1 and 7; BM(POE)$_2$: lanes 9 and 12]. Interestingly, crosslinking with 4F2hc mutants S151C and S412C was totally abolished when LAT2 Cys210 was mutated to serine (C210S) [Fig. 2*A*; BMOE, lanes 2 and 6; BM(POE)$_2$, lanes 8 and 11]. The C210S (LAT2) mutant is fully functional (i.e., heterodimerized (Fig. S2 *G* and *H*, lanes 2 and 4) and induced L-alanine transport with 4F2hc (Fig. S2*I*). In contrast, mutant C330S (Fig. 2*A*, lanes 5 and 10), and mutants S185C (Fig. 2*A*, lane 3) and S393C (Fig. 2*A*, lane 4) incorporated in this background did not show crosslinking with

wild-type LAT2. These results demonstrated specific crosslinking between cysteine residues at positions 151 or 412 (which are located in the loop Aα1–Aβ2 and helix Aα8′′′, respectively) of subdomain A of 4F2hc-ED and Cys210, which is located in the extracellular loop TMD5–6 in LAT2.

Docking Analysis of 4F2hc-ED and LAT2. To characterize the interactions between 4F2hc-ED and LAT2, protein-docking analyses between the atomic structure of 4F2hc-ED (8) and homology models of human LAT2 (Fig. S3*B*) were performed with only two restrictions: (*i*) allowing the formation of the disulfide bridge between residues Cys109 (4F2hc-ED) and Cys154 (LAT2), and (*ii*) avoiding clashes between 4F2hc-ED residues and the plasma membrane (*SI Methods*). Of 3,145 possible docking poses, the model with the lowest energy is depicted in Fig. 2*B*. According to this model, 4F2hc-ED interacts with all the extracellular loops or ends of TMDs of LAT2. 4F2hc is *N*-glycosylated in *Pichia* (18) and mammalian cells (8), and in the model the four putative sites are located in the most external face of 4F2hc-ED, out of the contact interface with LAT2 (Fig. 2*B*). There is a large interaction surface between the two proteins, with the buried surface area of LAT2 upon 4F2hc binding being 1,735 $Å^2$ (Fig. S4*A*). As much as 60% of the LAT2 interaction surface is formed by hydrophobic residues, and 40% is formed by aromatic residues. This composition is consistent with the major contribution of desolvation to the binding energy as calculated by our scoring function. The most important contacting residues are shown in Table S1 and Fig. S4*B*.

Interestingly, the lowest-energy 4F2hc-ED–LAT2 model complies with the crosslinking analysis described above. Thus, crosslinked residues S151C (4F2hc)–Cys210 (LAT2) and S412C (4F2hc)–Cys210 (LAT2) were located at minimal interatomic distances of 13.4 Å and 11.5 Å, respectively (Table S2). These distances are in good agreement with the results obtained from crosslinking with BMOE and $BM(POE)_2$, in which the distances separating both reactive maleimide ends range from 6.3 to 10.5 Å and from 3.5 to 14.3 Å, respectively (20). In contrast, the 4F2hc residues that did not crosslink, S393C and S185C, are located at distances of 18.8 Å and 28.2 Å, respectively, from LAT2 Cys210, also corroborating the docking model (Table S2). Then, guided by this docking model, additional cysteine mutants in protein domains not studied previously were considered for crosslinking, i.e., S195C in helix 2 of subdomain A and S487C and G505C in subdomain C of 4F2hc-ED and A235C, A315C, G392C, and S441C in four external loops of LAT2 (Table S2). To ascribe the crosslinked residues unequivocally, 4F2hc mutants were generated in C330S background, and LAT2 mutants were generated in the C210S background, taking advantage of the fact that LAT2 C210S heterodimerized with the newly considered His-4F2hc mutants (Fig. S5 *A* and *B*, lanes 7, 12, and 17) in HEK293T cells. Moreover, the rest of the additional 4F2hc and LAT2 mutants heterodimerized and induced L-alanine transport in the transfected cells (Fig. S5). Six new paired positions in 4F2hc and LAT2 were crosslinked by BMOE and/or $BM(POE)_2$ (Fig. 2*C* and Fig. S6 *A* and *B*). Interestingly, the new pairing of G505C (4F2hc) with A235C and S441C (LAT2) (Fig. 2*C*, lanes 6 and 7) and the already mentioned pairing of S151C and S412C (4F2hc) with Cys210 (LAT2) (Fig. 2*A*) crosslinked almost completely (80–95%) (Table S2). Together with the intersubunit disulfide bridge between Cys109 (4F2hc) and Cys154 (LAT2), which links >95% of the expressed LAT2 mutants to 4F2hc (Fig. S2*G*, lanes 1 and 3 and Fig. S5*A*, lanes 15 and 16), these results triangulate the location of 4F2hc-ED over the external face of LAT2 (Fig. 2*D*). Indeed, our crosslinking studies showed that four of the six external loops of LAT2 (Cys210 and Ala235 in TMD5–6, Ala315 in TMD7–8, Gly392 in TMD9–10, and Ser441 in TMD11–12) (Fig. S3, asterisks) are in the vicinity of residues in subdomains A and C of the 4F2hc-ED in addition to the intersubunit disulfide bridge connecting Cys154 in TMD3–4 of LAT2 and Cys109 located five residues away from the C-terminal end of the 4F2hc TMD (Fig. 2*D* and Table S2). According to the lowest-energy 4F2hc-ED–LAT2 model, all the crosslinked positions in the present work are 8.1–17.5 Å apart (Table S2). In contrast, paired positions separated by >15 Å or >18 Å were not crosslinked by BMOE or $BM(POE)_2$, respectively (Fig. 2*A*, Fig. S6*A*, and Table S2). The lack of crosslinking in the indicated paired positions was not caused by cysteine residues being blocked by the formation of a direct disulfide bridge as the result of very close proximity (Fig. S6 *B* and *C*). Thus, the lowest-energy docking model is in full agreement with all crosslinking experiments. Moreover, if a slightly larger crosslinking distance is considered, only two very similar additional docking solutions comply with the five strongest (≥60% efficiency) crosslinking experiments (Fig. S4*C*). Like the 3D 4F2hc/LAT2 map from TEM and SPA, these docking models place 4F2hc-ED tilted on top of LAT2. Unfortunately, at the resolution of 21 Å, the large volume of the larger domain in the map (Fig. 1*C*), which contains LAT2, the TMD and the N-terminal domain of 4F2hc, lipid, and detergent, precludes a reliable fitting of the 4F2hc-ED–LAT2 docking model into the 3D 4F2hc/LAT2 map. In summary, TEM, SPA, docking, and crosslinking studies strongly indicate that 4F2hc-ED is positioned tilted on LAT2, almost completely covering the extracellular face of the transporter.

The Ectodomain of the Heavy Subunit 4F2hc Increases the Stability of LAT2. The interaction between 4F2hc-ED and the overall external face of LAT2 suggests that the heavy subunit may affect the stability of the light subunit. To investigate this possibility, we studied the behavior of purified 4F2hc/LAT2 and LAT2. Solubilization with DDM of isolated membranes from yeast cells coexpressing His-4F2hc and Strep-LAT2 and sequential purification by Co^{2+}- and Strep-Tactin affinity chromatography yielded 4F2hc/LAT2 heterodimers (18). In contrast, DDM solubilization of yeast membranes expressing Strep-LAT2 alone and subsequent Strep-Tactin affinity chromatography and size-exclusion chromatography yielded only aggregates of LAT2 (Fig. 3*A*). To study whether 4F2hc was able to conserve the functionality of LAT2, we tried to reconstitute purified 4F2hc/LAT2 heterodimers into liposomes, but our attempts failed. As an alternative approach to test the functionality of 4F2hc/LAT2 heterodimers and LAT2 monomers, isolated *Pichia* membranes were solubilized in DDM and reconstituted into proteoliposomes. Interestingly, only 4F2hc/LAT2 heterodimers, but not LAT2 monomers, could be reconstituted successfully into proteoliposomes as functional proteins (Fig. 3*B*), because LAT2 monomers aggregated before being inserting into liposomes (Fig. S7*A*). Surprisingly, expression of Strep-LAT2 alone, as well as coexpression of His-4F2hc and Strep-LAT2, resulted in a similar transport of 10 μM L-leucine over background in *P. pastoris* cells (Fig. S7*B*). These results suggest that LAT2 is properly folded and trafficked to the plasma membrane in yeast cells. However, the interactions with 4F2hc would be essential to maintain the correct folding of the light subunit in detergent. Kinetic analysis of L-leucine transport via His-4F2hc/Strep-LAT2 and Strep-LAT2 revealed similar K_ms: 178 ± 15 μM and 120 ± 7 μM, respectively (Fig. S7*C*). Thus, the interaction between 4F2hc and the extracellular surface of LAT2 increased the stability of the detergent-solubilized light subunit but did not alter dramatically the substrate apparent affinity of this transporter in vivo.

Next, we asked whether the ectodomain of 4F2hc is able to stabilize LAT2 without the generation of the conserved disulfide bridge between both HAT subunits. *Pichia* membranes expressing Strep-LAT2 were incubated with purified His-4F2hc-ED, and then LAT2 was solubilized with different concentrations of DDM (Fig. 4*A*). Interestingly, preincubation with 4F2hc-ED, but not with same concentration of BSA, increased the solubilization of LAT2 at the three concentrations of detergent tested (1%, 0.5%, and 0.25% DDM). These results suggested that 4F2hc-ED stabilizes LAT2 in solution. To test this possibility, LAT2 solubilized in 1% DDM in the absence or presence of 4F2hc-ED was ultracentrifuged at 2 h, 24 h, and 72 h after solubilization. Remarkably, the presence of 4F2hc-ED dramatically prevented the

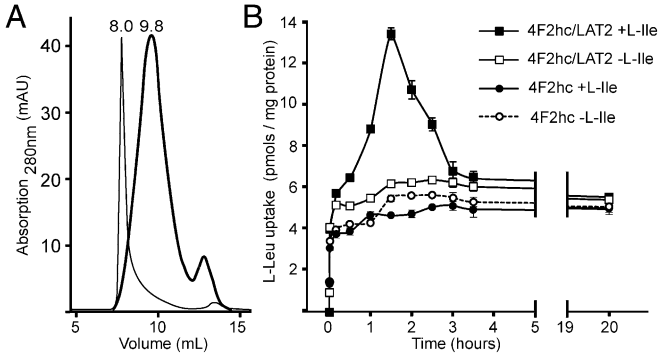

Fig. 3. (*A*) Size-exclusion chromatography profiles of purified 4F2hc/LAT2 (thick curve) and purified LAT2 (thin curve). 4F2hc/LAT2 elutes at 9.8 mL, whereas LAT2 is eluted in the void volume (8 mL). (*B*) Time-course of L-leucine uptake in 4F2hc/LAT2 and 4F2hc proteoliposomes. Transport of 10 μM L-[^{3}H]leucine into proteoliposomes was measured at 10, 30, 60, 90, 120, 150, 180, and 210 min and at 20 h. Proteoliposomes were loaded or not loaded with 4 mM cold L-isoleucine. Data are mean ± SEM of a representative experiment performed in triplicate. Transport of 10 μM L-[^{3}H]leucine into 4F2hc/LAT2 proteoliposomes preloaded with 4 mM L-isoleucine resulted in an overshoot. In contrast, L-leucine transport into 4F2hc/LAT2 proteoliposomes with no amino acids inside showed passive diffusion similar to that shown by 4F2hc proteoliposomes filled or not filled with L-isoleucine. This behavior is characteristic of coupled transporters such as the H^+/lactose cotransporter LacY (27) and exchangers such as the LAT transporter SteT, an L-serine/L-threonine exchanger from *Bacillus subtilis* (28).

precipitation of LAT2 (Fig. 4 *B* and *C*). In summary, these results indicate that the ectodomain of 4F2hc interacts with the external face of LAT2, thus increasing the stability of the detergent-solubilized transporter and allowing its functional reconstitution into proteoliposomes.

Discussion

This study reports on the supramolecular organization and the structural bases of the interactions of the heavy and light subunits of HATs. Specifically, three lines of evidence (TEM, SPA, and docking and crosslinking analyses) strongly support the notion that 4F2hc-ED almost completely covers the extracellular surface of the transporter subunit LAT2. Indeed, we identified specific residues that crosslinked 4F2hc and LAT2 nearly completely (>80%). This crosslinking, together with the endogenous intersubunit disulfide bridge, triangulates the position of the 4F2hc-ED over the external face of LAT2 (Fig. 2*D*). Importantly, the proposed docking model, as well as two additional and highly similar poses, fulfills the steric restrictions defined by the results from crosslinking (Fig. S4*C*).

Our docking analysis used the atomic structure of human 4F2hc-ED and homology models of human LAT2 based on the atomic structure of the amino acid transporter AdiC in an outward-facing conformation. Because of the low sequence conservation in the loops of AdiC and LAT2 (Fig. S3*A*), our docking models do not represent high-resolution structures of the 4F2hc-ED–LAT2 complex. Nevertheless, docking analysis revealed desolvation as the main contributor to the binding energy of 4F2hc-ED and LAT2. Indeed, the LAT2 residues that are predicted to be more relevant for the interactions are mainly hydrophobic, and they can be grouped into two clearly defined patches [see Normalized Interface Propensity (NIP) residues in Table S1 and Fig. S4 *A* and *B*]. One of the patches, which is totally hydrophobic, is composed of nine residues distributed along three external loops or TMD ends of LAT2 (TMD3–4, which harbors the Cys154 residue involved in the disulfide bridge, TMD9–10, and TMD11–12). The other is a mixed patch composed of four polar and five hydrophobic residues located in loops TMD1–2, TMD5–6, and TMD7–8. The interaction between 4F2hc-ED and LAT2 raises the question of whether the heavy subunit might have an impact on the LAT2 transport cycle. The structural paradigms of HAT light subunits, the bacterial APC transporters, present the LeuT-fold (14–17). Secondary transporters, upon the binding of an external substrate, transit to inward-facing conformations to release the substrate inside the cell. Besides transporter-specific changes, atomic structures of LeuT-fold transporters showed a commonality of features in this transition (21, 22): the "hash" domain (TMDs 3, 4, 8, and 9) and the extracellular ends of the "bundle" domain (TMDs 1, 2, 6, and 7) become closer, and the loop TMD7–8 occludes the external vestibule of the transporter. Our results indicate that these conformational changes are compatible with 4F2hc-ED directly contacting the external loops or ends of TMDs of LAT2. The highly conserved hydrophobic patch in LAT2 (Fig. S4*B* and Table S1), together with the intersubunit disulfide bridge, glue the hash domain and TMDs 11 and 12 to 4F2hc-ED. TMDs 11 and 12 are, according to the structural homolog AdiC (17), the most static TMDs. In contrast, the mixed patch is less conserved and involves the bundle domain and the occluding loop (TMD7–8). This architecture suggests that 4F2hc/LAT2, and probably other HATs, have evolved to bind the ectodomain of the heavy subunit firmly to the hash domain. In this scenario, energetically similar interactions of 4F2hc-ED with the bundle domain and loop TMD7–8 would be broken and replaced by the different conformations that the light subunit undergoes during the transport cycle.

According to amino acid transporters with LeuT-fold, the substrate-binding site in LAT2 is expected to be located at the bottom of the extracellular vestibule (1, 13) and therefore far away from the interacting 4F2hc-ED residues (Fig. S4 *D* and *E*). Moreover, our docking analysis located 4F2hc-ED in a tilted

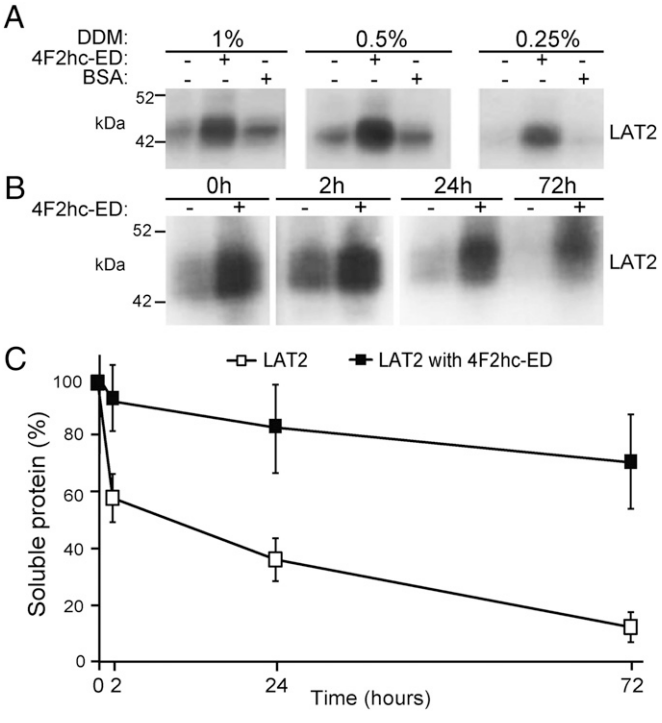

Fig. 4. 4F2hc-ED increases LAT2 solubility and stability. (*A*) Western blot analysis of DDM-solubilized LAT2 in the presence of 1 mg/mL of 4F2hc-ED or BSA or plain buffer, as indicated. (*B*) Western blot analysis of solubilized LAT2 (1% DDM) in the presence or absence of 1 mg/mL of 4F2hc-ED at different times. (*C*) Quantification of the soluble LAT2 at the indicated time. Data are the mean ± SEM of three independent experiments as described in *B*. LAT2 remaining in solution after ultracentrifugation was considered soluble LAT2. LAT2 was detected using αStrep antibody. The presence of 4F2hc-ED increased LAT2 stability at all analyzed times.

position, with subdomain C interacting with LAT2 TMD11–12 and leaving open a window in the opposite location flanked by LAT2 TMD7–8 for the entrance of the substrate to the binding site (Fig. S4*D*). Despite the different structures of the LAT2 monomer and the 4F2hc/LAT2 heterodimer, the measured K_m values for L-leucine transport in *Pichia* cells were comparable, suggesting that 4F2hc would have no significant impact on the substrate affinity of LAT2.

The hydrophobic character of the interaction between 4F2hc-ED and LAT2 might be the basis for the stabilization of this light subunit by 4F2hc. We show that 4F2hc allows functional reconstitution into proteoliposomes and purification of the transporter after solubilization with DDM. Moreover, we show here that 4F2hc-ED suffices to increase the stability of DDM-solubilized LAT2. The binding of 4F2hc-ED to the extracellular surface of LAT2 would bury a large hydrophobic patch that otherwise would be exposed to solvent, thus reducing aggregation and increasing stability. In addition, the compact and thermally stable structure (T_m ~59 °C) (23) of 4F2hc-ED may have additional effects in improving LAT2 stability.

HATs appeared in metazoans with an ancient heavy subunit that evolved to differentiated 4F2hc and rBAT in vertebrates (1). The fact that LAT2 monomers elicited amino acid transport in *Pichia* cells, which do not express 4F2hc or related proteins, indicates that 4F2hc is not required for proper folding of LAT2, as also has been demonstrated for the light subunit $b^{0,+}$AT in the absence of rBAT (2). In contrast, 4F2hc and rBAT are necessary for heterodimerization and functional expression of light subunits at the cell surface when expressed in *Xenopus* oocytes and mammalian cells (1). Specifically, 4F2hc-ED is necessary for these functions (9, 10). Desolvation of hydrophobic residues might be extended to the recognition of other light subunits by 4F2hc. The hydrophobic NIP residues in our docking analysis are highly conserved in 4F2hc-associated light subunits but are poorly conserved in cyanobacterial, yeast, and fungal LATs, which are the closest homologs to vertebrate LATs (up to 37% amino acid sequence identity) that do not interact with a heavy subunit (Table S1). Hydrophobic NIP residues also are largely conserved in $b^{0,+}$AT (Table S1). Thus, desolvation of hydrophobic residues also might contribute to the binding of the ectodomain of rBAT and its light subunit. Indeed, cotransfection of 4F2hc and $b^{0,+}$AT (i.e., the rBAT-associated light subunit) in mammalian cells yielded functional transporter at the cell surface (24). Interaction through a hydrophobic patch seems like a clever way to glue 4F2hc to six different light subunits (LAT1, LAT2, y^+LAT1, y^+LAT12, asc1, and xCT) that share as little as ~43% amino acid sequence identity (1). Our work revealed that 4F2hc-ED covers the external face of LAT2, increasing transporter stability. The idea that a common hydrophobic patch serves for subunit recognition by 4F2hc merits future experimental examination.

Methods

The indicated tagged versions of human 4F2hc and LAT2 were expressed and purified as reported previously (18). L-leucine transport by *Pichia* cells was performed as described (18). Transport activity of LAT2, 4F2hc, and 4F2hc/LAT2 was tested as described previously (13) by measuring their L-leucine/L-isoleucine exchange activity in reconstituted proteoliposomes. TEM, SPA, and 3D reconstruction were performed as described in *SI Methods*. Docking calculations of 4F2hc-ED–LAT2 interaction were performed based on the pyDock protocol (25), and the most relevant LAT2 residues for the interaction with 4F2hc were identified by using the NIP value (26). To validate the docking model, intersubunit crosslinking was performed in different versions of purified 4F2hc/LAT2 heterodimer expressed in HEK cells. The effect of 4F2hc-ED on the detergent solubilization and stability of human LAT2 was tested by incubating *Pichia* membranes expressing LAT2 (18) with purified 4F2hc-ED (8) before solubilization with DDM. Soluble LAT2 protein was detected and quantified by Western blotting. See *SI Methods* for details.

ACKNOWLEDGMENTS. This work was supported by Spanish Ministry of Science and Innovation Grants BIO2010-22324 (to J.F.-R.) and SAF2012-40080-C02-01, European Commission Frame Program 7 Grant 201924 (European Drug Initative on Channels and Transporters), Fundación Ramón Areces, and the Generalitat de Catalunya Grant SGR2009-1355 (to M.P.); by University of Bern, Swiss National Science Foundation Grants 31003A_125150 and 31003A_144168; the Bern University Research Foundation; the Novartis Foundation; the Marie Curie Actions International Fellowship Program; and National Center of Competence in Research TransCure (D.F.).

1. Fotiadis D, Kanai Y, Palacín M (2013) The SLC3 and SLC7 families of amino acid transporters. *Mol Aspects Med* 34(2-3):139–158.
2. Reig N, et al. (2002) The light subunit of system b(o,+) is fully functional in the absence of the heavy subunit. *EMBO J* 21(18):4906–4914.
3. Feliubadaló L, et al.; International Cystinuria Consortium (1999) Non-type I cystinuria caused by mutations in SLC7A9, encoding a subunit ($b^{o,+}$AT) of rBAT. *Nat Genet* 23(1):52–57.
4. Mastroberardino L, et al. (1998) Amino-acid transport by heterodimers of 4F2hc/CD98 and members of a permease family. *Nature* 395(6699):288–291.
5. Rius M, Chillarón J (2012) Carrier subunit of plasma membrane transporter is required for oxidative folding of its helper subunit. *J Biol Chem* 287(22):18190–18200.
6. Fernández E, et al. (2006) The structural and functional units of heteromeric amino acid transporters. The heavy subunit rBAT dictates oligomerization of the heteromeric amino acid transporters. *J Biol Chem* 281(36):26552–26561.
7. Feral CC, et al. (2005) CD98hc (SLC3A2) mediates integrin signaling. *Proc Natl Acad Sci USA* 102(2):355–360.
8. Fort J, et al. (2007) The structure of human 4F2hc ectodomain provides a model for homodimerization and electrostatic interaction with plasma membrane. *J Biol Chem* 282(43):31444–31452.
9. Fenczik CA, et al. (2001) Distinct domains of CD98hc regulate integrins and amino acid transport. *J Biol Chem* 276(12):8746–8752.
10. Bröer A, et al. (2001) Association of 4F2hc with light chains LAT1, LAT2 or y+LAT2 requires different domains. *Biochem J* 355(Pt 3):725–731.
11. Gasol E, Jiménez-Vidal M, Chillarón J, Zorzano A, Palacín M (2004) Membrane topology of system x_c^- light subunit reveals a re-entrant loop with substrate-restricted accessibility. *J Biol Chem* 279(30):31228–31236.
12. Jiménez-Vidal M, et al. (2004) Thiol modification of cysteine 327 in the eighth transmembrane domain of the light subunit xCT of the heteromeric cystine/glutamate antiporter suggests close proximity to the substrate binding site/permeation pathway. *J Biol Chem* 279(12):11214–11221.
13. Bartoccioni P, et al. (2010) Role of transmembrane domain 8 in substrate selectivity and translocation of SteT, a member of the L-amino acid transporter (LAT) family. *J Biol Chem* 285(37):28764–28776.
14. Shi Y (2013) Common folds and transport mechanisms of secondary active transporters. *Annu Rev Biophys* 42:51–72.
15. Shaffer PL, Goehring A, Shankaranarayanan A, Gouaux E (2009) Structure and mechanism of a Na+-independent amino acid transporter. *Science* 325(5943):1010–1014.
16. Fang Y, et al. (2009) Structure of a prokaryotic virtual proton pump at 3.2 Å resolution. *Nature* 460(7258):1040–1043.
17. Kowalczyk L, et al. (2011) Molecular basis of substrate-induced permeation by an amino acid antiporter. *Proc Natl Acad Sci USA* 108(10):3935–3940.
18. Costa M, et al. (2013) Expression of human heteromeric amino acid transporters in the yeast *Pichia pastoris*. *Protein Expr Purif* 87(1):35–40.
19. Jastrzebska B, et al. (2011) Rhodopsin-transducin heteropentamer: Three-dimensional structure and biochemical characterization. *J Struct Biol* 176(3):387–394.
20. Green NS, Reisler E, Houk KN (2001) Quantitative evaluation of the lengths of homobifunctional protein cross-linking reagents used as molecular rulers. *Protein Sci* 10(7):1293–1304.
21. Shimamura T, et al. (2010) Molecular basis of alternating access membrane transport by the sodium-hydantoin transporter Mhp1. *Science* 328(5977):470–473.
22. Krishnamurthy H, Gouaux E (2012) X-ray structures of LeuT in substrate-free outward-open and apo inward-open states. *Nature* 481(7382):469–474.
23. Turnay J, et al. (2011) Structural characterization and unfolding mechanism of human 4F2hc ectodomain. *Biochim Biophys Acta* 1814(5):536–544.
24. Rajan DP, et al. (2000) Differential influence of the 4F2 heavy chain and the protein related to b(0,+) amino acid transport on substrate affinity of the heteromeric b(0,+) amino acid transporter. *J Biol Chem* 275(19):14331–14335.
25. Cheng TM, Blundell TL, Fernandez-Recio J (2007) pyDock: Electrostatics and desolvation for effective scoring of rigid-body protein-protein docking. *Proteins* 68(2):503–515.
26. Fernández-Recio J, Totrov M, Abagyan R (2004) Identification of protein-protein interaction sites from docking energy landscapes. *J Mol Biol* 335(3):843–865.
27. Newman MJ, Foster DL, Wilson TH, Kaback HR (1981) Purification and reconstitution of functional lactose carrier from *Escherichia coli*. *J Biol Chem* 256(22):11804–11808.
28. Reig N, et al. (2007) Functional and structural characterization of the first prokaryotic member of the L-amino acid transporter (LAT) family: A model for APC transporters. *J Biol Chem* 282(18):13270–13281.